Computers & Geosciences 106 (2017) 89–100

Contents lists available at ScienceDirect

Computers & Geosciences

journal homepage: www.elsevier.com/locate/cageo

Research paper

Applicability of computer-aided comprehensive tool (LINDA: LINeament Detection and Analysis) and shaded digital elevation model for characterizing and interpreting morphotectonic features from lineaments

Alaa Masoud[a,*], Katsuaki Koike[b]

[a] Geology Department, Faculty of Science, Tanta University, 31527 Tanta, Egypt
[b] Department of Urban Management, Graduate School of Engineering, Kyoto University, Kyoto 615-8540, Japan

ARTICLE INFO

Keywords:
DEM shading
Segment Tracing Algorithm
Segment grouping
Fault geometry estimation
Eastern Desert (Egypt)

ABSTRACT

Detection and analysis of linear features related to surface and subsurface structures have been deemed necessary in natural resource exploration and earth surface instability assessment. Subjectivity in choosing control parameters required in conventional methods of lineament detection may cause unreliable results. To reduce this ambiguity, we developed LINDA (LINeament Detection and Analysis), an integrated tool with graphical user interface in Visual Basic. This tool automates processes of detection and analysis of linear features from grid data of topography (digital elevation model; DEM), gravity and magnetic surfaces, as well as data from remote sensing imagery. A simple interface with five display windows forms a user-friendly interactive environment. The interface facilitates grid data shading, detection and grouping of segments, lineament analyses for calculating strike and dip and estimating fault type, and interactive viewing of lineament geometry. Density maps of the center and intersection points of linear features (segments and lineaments) are also included. A systematic analysis of test DEMs and Landsat 7 ETM+ imagery datasets in the North and South Eastern Deserts of Egypt is implemented to demonstrate the capability of LINDA and correct use of its functions. Linear features from the DEM are superior to those from the imagery in terms of frequency, but both linear features agree with location and direction of V-shaped valleys and dykes and reference fault data. Through the case studies, LINDA applicability is demonstrated to highlight dominant structural trends, which can aid understanding of geodynamic frameworks in any region.

1. Introduction

Earth surface and subsurface fractures represented by lineaments play essential role in natural resources exploration and susceptibility hazard mapping of earthquakes/landslides (e.g., Rowland and Sibson, 2004; Masoud and Koike, 2006). Properties of lineaments such as extent, density, intersection, and orientation have proven major indicators of zones of high permeability and/or low pressure that may act as pathways for fluid- and gas-related resource migration. Lineaments may represent faults that control basin development and the distribution of reservoirs (Warner, 1997). Regional lineaments are commonly interpreted as surface expressions of geologic weak zones at tectonic boundaries of basins and plates, as well as of faults and rock fractures (e.g., Oakey, 1994; Fichler et al., 1999; Kudo et al., 2004; Milbury et al., 2007; Austin and Blenkinsop, 2008).

Large-scale characterization of geologic structures and tectonics has been supported by recent advances in computer hardware and spatial analysis techniques (e.g., Masoud and Koike, 2011a, 2011b). A number of algorithms have been developed for automatic or semi-automatic detection of lineaments related to geologic structures (see Ramli et al. (2010) for a review). Recent advances in the automated techniques enable detection of changes in lineament patterns (Soto-Pinto et al., 2013). The semi-automatic techniques have proven capabilities for mapping tectonic lineaments similar to photointerpretation (Vaz et al., 2012), characterizing geologic lineaments by a 3D approach using DTM curvature values (Bonetto et al., 2015), and mapping large-scale geologic structures and calculating their dip angles and directions from analysis of photogrammetric data acquired by Unmanned Aerial Vehicles (Vasuki et al., 2014).

Many methods of automatic and semi-automatic extraction of lineaments from grid data such as satellite images and digital elevation models (DEMs) are mostly based on edge-detection techniques using spatial and morphological filters (e.g., Süzen and Toprak, 1998; Tripathi et al., 2000; Soto-Pinto et al., 2013). Frequency and con-

* Corresponding author.
E-mail address: alaa_masoud@science.tanta.edu.eg (A. Masoud).

http://dx.doi.org/10.1016/j.cageo.2017.06.006
Received 19 January 2017; Received in revised form 5 June 2017; Accepted 6 June 2017
Available online 09 June 2017
0098-3004/

nectivity of the lineaments are strongly affected by the scale of the source grid data and detection parameters when filters are applied (Argialas and Mavrantza, 2004). Therefore, plausible representation of tectonically significant lineaments relevant to faults and long rock fractures cannot be realized. It is indispensable then to develop an automated technique that can enhance the frequency and connectivity of detected lineaments so that resultant lineament maps resemble actual fault maps.

Additionally, selection of suitable data sources for autodetection of tectonically significant lineaments is important. Satellite images representing reflectance and backscattering characteristics of the earth surface in response to electromagnetic waves at various wavelengths are generally used for lineament extraction. However, artificial linear features unrelated to fractures, such as boundaries of land use and land cover, also tend to be detected in satellite images. Precise DEM data can be used to avoid such misdetection. Results can be made more effective by the combined use of grid data from multiple sources that encompass wide compositional variations of subsurface geophysical attributes (e.g., gravity and magnetic) and depth variation represented by topography, especially when integrated at various scales. This can improve understanding of the relationship between tectonic trends and anomalies that develop at varying depths and geological discontinuities (Masoud and Koike, 2011a, 2011b).

Although automated or semi-automated software for efficient detection and analysis of linear features are indispensable, most are presently commercial and need subjective setting of detection parameters. Reproducibility of features with optimal accuracy is largely not achievable. Development of freely accessible software for automated mapping of linear features is therefore essential.

Based on the above background, publicly available software is needed that can implement automatic lineament detection, analyses, and visualization within a user-friendly interface, using multiple sources of grid data. Toward this, we developed Visual Basic software LINDA (LINeament Detection and Analysis), which is exclusively menu-driven and customized for operation on PCs. The general terms “segment”, “lineament”, and “linear feature” are used in LINDA to indicate one line, a group of collinear segments, and topographic feature that includes both segment and lineament, respectively. Software with the same acronym (LINDA: Linear-feature Network Detection and Analysis) was developed by Wang (1993) to mainly detect roads, stream networks, and boundaries of features from remotely sensed data; this is not related to our LINDA software. Our LINDA software has several options, namely, enhancing, detecting, and grouping segments into one lineament, calculation of strike and dip, estimation of fault type, point density mapping, and visualization of lineaments and their geometry. These functions are more comprehensive and advanced than those of preceding and few open software of lineament analysis such as Raghavan et al. (1995), Abarca (2006), and Šilhavý et al. (2016). Results of applying LINDA to a dataset of DEM and LANDSAT ETM+ imagery in the North and South Eastern Desert of Egypt are presented for demonstrating the software performance and effectiveness of multi-shaded DEM. Although LINDA is essentially an integration of the authors’ published methods, it has new function to discriminate linear features from dykes and valleys as below-mentioned. In addition, this study reveals suitability of DEM and satellite imagery for lineament analysis and detailed characterization of fracture system.

2. Flow and main tools of LINDA

The main tools of LINDA summarized below are based on algorithms for enhancement of line features in grid data, identification and grouping of segments, normal vector calculation of topographic surfaces, calculation of fracture- or fault-related plane orientation by vector analysis, and fault-type modeling. These main tools were developed using Fortran 90 and Visual Basic (VB) 6.0 code. Because

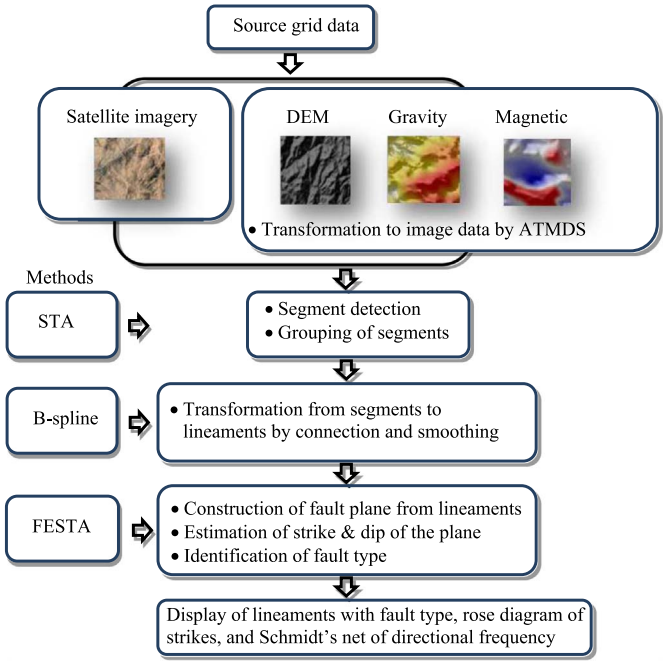

Fig. 1. Structure of major functions of LINDA and flow of data analyses toward visualization of the results.

the Fortran 90 code was faster to execute than VB, we developed hybrid coding with graphical user interface (GUI) in VB, and Fortran 90 executable files were then called from the VB code. Fig. 1 shows a flowchart of the processing of input data. Major merit of GUI in VB is that it enables interactive integrated analyses of multi-source data.

Shading intensity of grid data (any data except for imagery) varies with illumination azimuth and tilt (Fig. 2). LINDA adopts an adaptive-tilt, multi-directional shading (ATMDS: Masoud and Koike, 2011a) that illuminates grid data along six azimuths at 30° intervals and upward tilt angles 0–45° and selects the maximum intensity at each point.

A segment tracing algorithm (STA: Koike et al., 1995) is a core for detection of linear features by examining local variance of DEM shade intensity and satellite imagery, identifying line elements by the secondary differential, and connecting them along the minimum variance directions. Segments are then grouped based on collinearity angle 10° and distance (Masoud and Koike, 2011a) and concatenated into one long lineament with strike vector $\boldsymbol{d}$ using a B-spline (BSP). This distance is dependent upon the spatial resolution of the grid data assigned as the grid spacing multiplied by the number of pixels along x and y directions set also as the grid spacing by default, i.e., the distance becomes equal to the grid spacing of 30 m x 30 pixels which is equal to 900 m in our case studies.

A lineament is assumed to be a trace of fracture/fault plane with normal vector $\boldsymbol{n}$ on the ground with normal vector $\boldsymbol{t}$. Then, the unknown $\boldsymbol{n}$ can be calculated by the relationship $\boldsymbol{d} = \boldsymbol{t} \times \boldsymbol{n}$ (Koike et al., 1998). The dip-directional relationship between $\boldsymbol{n}$ and $\boldsymbol{t}$ is used to judge the interpreted fault feature, i.e., the same (normal), opposite (reverse), or undetermined (strike-slip) (Masoud and Koike, 2011a). Essences of STA, BSP, the calculation method of $\boldsymbol{n}$, and the fault type judgement are briefly described in Supplementary data.

A combination of the above two techniques, FESTA (Fracture/fault-plane orientation and type Estimation with STA), is applicable to gravity and magnetic lineaments that represent narrow, low-anomaly zones, because of planes likely associated with faulting of different styles and types of movement. Although comprehensive field measurements are necessary for assigning tectonic significance to each lineament, they are laborious and time-consuming and are not globally achievable. In addition to a DEM, multiple data sources are needed for

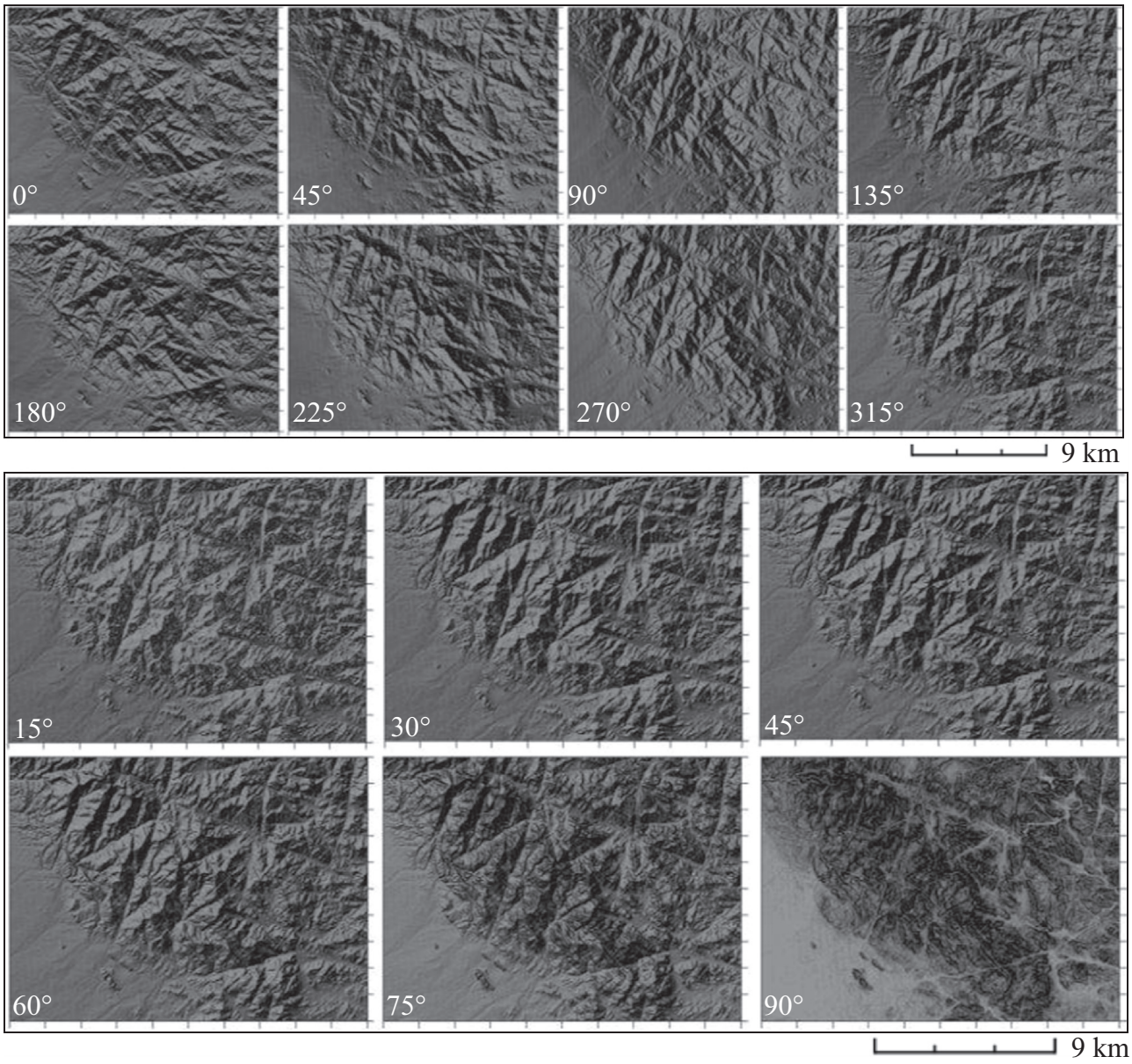

Fig. 2. Shades at several azimuths from 0° to 315° (top; angle is clockwise from west) and tilt angles from 15° to 90° (bottom) of illumination source, from test DEM of southwestern Sinai Peninsula in Egypt covering 18 km × 18 km area, showing bias of topographic features dependent on illumination direction.

such tectonic verification in a study area. Therefore, the interpreted fault plane orientation/type from our techniques are preliminary and need detailed user validation using local specific field-based geologic structural data.

3. Software description

LINDA is programmed in VB and runs on Microsoft Windows (XP and later). Calculation cores are prepared in Fortran 90 and called from the program menu in VB. For user-friendliness and productivity, LINDA results are interpreted via the user interface (Fig. 3). GUI is standalone and point and click, which enables the user to perform rapid, rigorous, and interactive detection and analysis of linear feature data. The GUI includes a wide range of plots for visual inspection of segments/lineaments and points of segment centers and intersections. GUI components of LINDA are explained in Appendix A.

LINDA is composed of various data processing and rendering tools. A range of analysis options is available from the menu bar. For each analysis, the process runs in the background with a Fortran 90 console that closes when the task is completed. Data processing can run in stepwise fashion or in sequential single step, including shading, segment detection, grouping of segments for transformation to lineaments, normal vector calculation to determine the strike and dip of planes, and fault-type modeling. The function of point analysis is to locate the centers and intersection points of segments/lineaments. On completion of this analysis, results are output to a specified text file through which the user can manipulate and/or visualize the results. For this visualization, a form is loaded and user-defined rendering options can be selected. Rendering of segments and lineaments is achieved through the generation of rose diagrams and Schmidt nets (lower hemisphere projection) for the strike and dip of lineaments, respectively. Appendix A explains the submenus implemented in LINDA.

3.1. Input/output data

LINDA's input/output file formats are shown in Table 1. Grid data including topography, gravity, magnetic, and grayscale values of

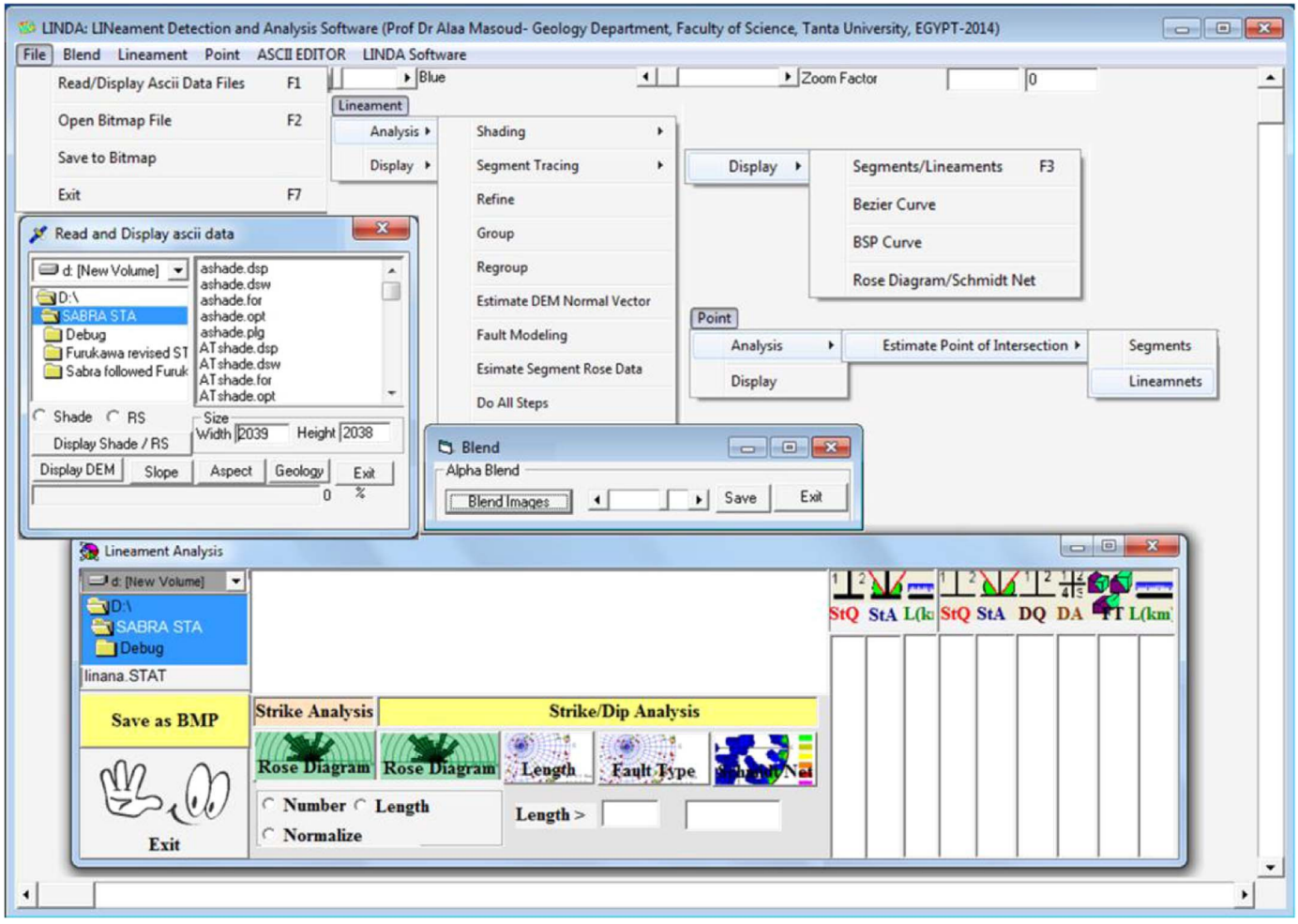

Fig. 3. GUI of LINDA main components.

reflectance and backscatter intensity from satellite bands are stored in ASCII file format, with digital numbers across columns and rows. Use of the first three types of grid data was demonstrated in Masoud and Koike (2011a). The other input and output files are usual text style and their filename extensions are abbreviations of the data contents. Input data are projected on the two-dimensional Cartesian coordinate system of Universal Transverse Mercator (UTM) conformal projection with World Geodetic System (WGS 84) ellipsoid. The selection of this projection is justified by its close similarity to the image Cartesian coordinate system, which facilitates accurate and easy conversion of the results to widely used GIS formats.

The file begins with a header line defining the data dimension by numbers of columns and rows and grid spacing along the x and y directions. Standard text files are used for parameter files and storing data of segments/lineaments, normal vectors of planes, fault type, and point centers and intersections. The segment file stores the number of segments on the first line, followed by the start (x_1, y_1) and end (x_2, y_2) point coordinates of each segment. The lineament file is headed by the

Table 1
Main functions of LINDA; input, output, and parameter files required for each function; and variables in each parameter file.

Process	Input file (s)	Output file (s)	Variables in parameter file					
Shading	DEM.asc	*.shd	NX	NY	DX	DY	Interval°	
STA	*.sh DEM.asc	*.seg	*.sh	*DEM.asc	*.seg			
Refinement	*.seg	*.rseg						
Grouping	*.seg	*.grp	*.seg	*.grp	DX	DY	Interval°	
Regrouping	*.grp	*.rgrp						
FESTA	DEM.asc	*.norm	NY	NX	DX	DY		
Lineament	*.grp DEM.asc *.norm	*. STAT *. FSN *. BSP	*.grp	*.dem	*.norm	*. STAT	*. FSN	*. BSP
Point	*.seg *.grp	*.splc *.gplc *.gpoi	DX	DY	*.seg *.grp	*.splc *.gplc	*.spoi *.gpoi	

NB: *Processes in Italics are optional.* * indicates a file name defined by user. NX and NY represent number of grid points along x and y axes, and DX and DY are grid intervals. Interval in shading is in degrees from west and interval in grouping is angle of collinearity.

total number of groups, followed by a list of the group number, number of segments in the group, and start and end point coordinates of each segment. The file of analysis results lists the serial number of the group, strike azimuth code (1 = NW and 2 = NE), strike angle, dip direction code (1 = NW, 2 = NE, 3 = SE, and 4 = SW), dip angle, fault type (1 = normal, 2 = reverse, and 3 = strike-slip), and lineament length in kilometers. Point data are stored as their Cartesian image coordinates. To enable integration and validation of the results from various data sources, the grid data should have the same coordinate system and grid spacing. Coordinate transformation can be achieved by resampling the data using the *VTBuilder* tool of the Virtual Terrain Project, which is freely available at http://vterrain.org/.

3.2. Visualization of results

The distribution and orientation of resultant segments and lineaments can be visualized as a map, rose diagram, or Schmidt net. Lineament maps can interactively display the number of segments in the group with the strike and dip, using BSP techniques. The Bézier curve is used to smooth lineaments and display them without strike/dip data. Fault types and their frequencies are displayed with the Schmidt net, in addition to pole orientations of the fracture- or fault-related planes. Shades from the grid data are blended with color-coded grid data to generate a plausible terrain appearance. Shade and blend maps can be used as backgrounds when displaying the segments/lineaments and point features.

4. Verification results of LINDA and multi-shaded DEM

The applicability and usefulness of LINDA and multi-shaded DEM were tested for two areas in the Eastern Desert of Egypt. The DEM data were taken from the Shuttle Radar Topography Mission (SRTM), and Landsat 7 ETM+ imagery was used for comparison with the DEM lineaments. Spatial resolution of the DEM used (SRTM-1 DEM with grid spacing 30 m) and Landsat 7 image are the same. Original six-band images from visible to short-wave infrared regions (bands 1–5 and 7: B1–5 and B7), which are composed of digital numbers of 8-bit scale (0–255) at each pixel, were used without radiometric enhancement in LINDA. Selection of the two areas was based on their unique geologic features, clear structural features appearing on aerial photographs and remotely-sensed imagery, and availability of reference structural data from field surveys.

4.1. Detection of dykes versus valleys

The first case study targeted the Hawashiya region in the extreme northern part of the Eastern Desert, west of Ras Gharib city on the Red Sea coast of Egypt (Fig. 4; size 29 km × 20 km). Band 1 imagery was selected for analysis when it proved advantageous in terms of frequency of segments detected over all bands (Section 4.2). The prime objective was to evaluate LINDA's capability to detect and characterize linear features associated with the dykes (convex topography) and discriminate them from those associated with valleys of V-shaped (concave) topography. In the Hawashiya region, calc-alkaline dyke swarms and mafic and felsic dykes are distributed in continental crust that formed rapidly under extensional tectonic settings and intruded into Neoproterozoic rocks composed of high-relief granites and low-relief older granitoids (Stern et al., 1984; Dawoud et al., 2006). The dykes were generated in the rift-related igneous activity and formed mostly by liquid immiscibility, fractional crystallization, and crustal anatexis of rhyolitic and andesitic magmas (Stern and Voegeli, 1987). Locations of the major faults and dykes were referred to Nossair (1987).

Linear features detected in the V-shaped valleys and dykes were discriminated by a threshold curvature derivative of the DEM. Negative curvature designated a valley feature and a positive one a dyke feature.

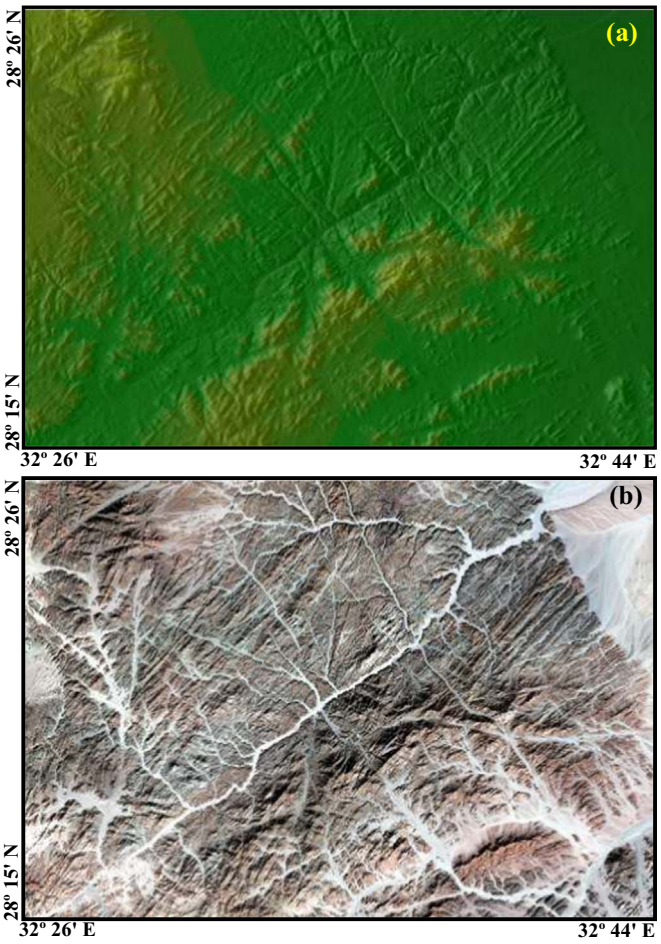

Fig. 4. Color-coded DEM blended with multi-shaded relief image (a) and natural color composite of Landsat 7 ETM+ imagery (b) for first case study in the extreme northern part of the Eastern Desert (west of Ras Gharib city on Red Sea coast of Egypt). (For interpretation of the references to color in this figure legend, the reader is referred to the web version of this article.)

Table 2
Counts of linear features, segments (Seg) and lineaments (Lin), along V-shaped valleys and dykes detected from multi-shaded DEM and Landsat ETM+ band 1 image for first case study area, North Eastern Desert in Egypt.

Topographic feature	V-shaped valleys				Dykes			
Data source	DEM		Image		DEM		Image	
Line feature	Seg	Lin	Seg	Lin	Seg	Lin	Seg	Lin
Count	**8663**	**1354**	**7608**	**1179**	**6752**	**954**	**6737**	**2405**

Both numbers of segments and lineaments were larger from the DEM use than the image use (Table 2). LINDA results from the DEM use are depicted by (a) segments over the shaded and colored DEM, (b) Bézier-smoothed lineaments, (c) BSP-smoothed lineaments with putative fault types, (d) distribution of the poles of interpreted fracture- or fault-related planes with fault types, (e) pole density (directional frequencies of the planes) using the Schmidt nets, and (f) rose diagram (Fig. 5). The blended map was used as background for verifying the positional and directional accuracy of the algorithms used and their resulting segments and lineaments. Fig. 6 shows the same expressions for the result of B1 image use. The general dominant trends and the qualitative spatial distribution of the linear features extracted by LINDA respect the linear geological elements from literature (e.g., Nossair, 1987).

In the study area, 8663 segments associated with continuous V-shaped valleys were detected from the DEM and grouped into 1354

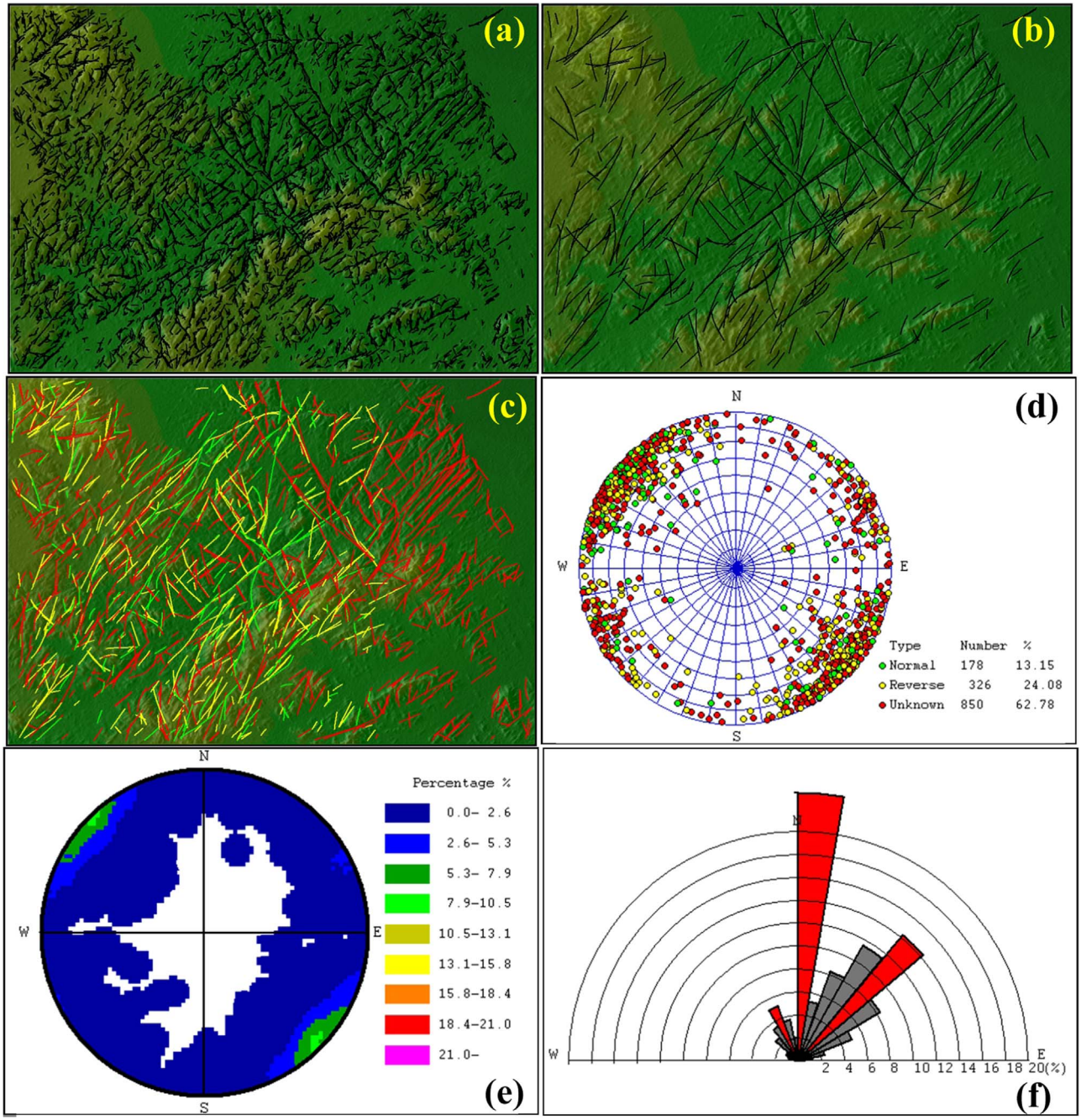

Fig. 5. Flow of LINDA using DEM data of study area (Fig. 4a): (a) Segments overlaid on shades blended with colored DEM; (b) Bézier-smoothed lineaments; (c) BSP-smoothed lineaments with fault types (yellow: normal, green: reverse, and red: strike-slip); (d) distribution of poles of interpreted fracture- or fault-related planes with fault types; (e) pole density using Schmidt nets (lower hemisphere projection); (f) rose diagram for strikes of lineaments. Sectors of trends are colored red, as in Figs. 6 and 7 (For interpretation of the references to color in this figure legend, the reader is referred to the web version of this article.).

lineaments. The morphotectonic control on the V-shaped valleys topography had been demonstrated (e.g., Goren et al., 2014; Roy and Sahu, 2015; Wołosiewicz, 2016). The lineaments highlighted prevailing N–S, NE, and N–W trends in decreasing order of dominance. For fault type, more than half the lineaments are dominated by strike-slip (63%) type, followed by reverse (24%) and normal (13%) types. Both the detected segments (7608) and grouped lineaments (1179) are smaller in the B1 image use, but the dominant directions of lineaments and frequencies of fault types are similar to those in the DEM results. Owing to a lack of the reference reports of geologic structure in the test area, the fault types were not quantitatively validated but qualitatively interpreted based on similarity of directional properties by Nossair (1987). That work specified three predominant fault trends affecting the various rock exposures, NE, N–S, and NW, with the NE trend the youngest. Additionally, aeromagnetic surveys and analysis of total magnetic intensity identified four main structural trends, N-S, NW, NE, and E–W. These correspond to the Dead Sea transform fault accompanying strike-slip, Gulf of Suez and Red Sea rifting, the Trans-African lineament, and Najd Fault system, respectively (Hassanein and Soliman, 2008; Masoud and Koike, 2011b). The reported trends of faults and magnetic intensity are the strongest in the N–S trend, followed by NE and NW. This coincides with the DEM result.

The dykes were also detected well from both the DEM and B1 images, and the locations and distributions of these dykes from the two data sources were in agreement (Fig. 7). The numbers of lineaments likely related to long dykes are 954 from DEM use and 2405 from B1

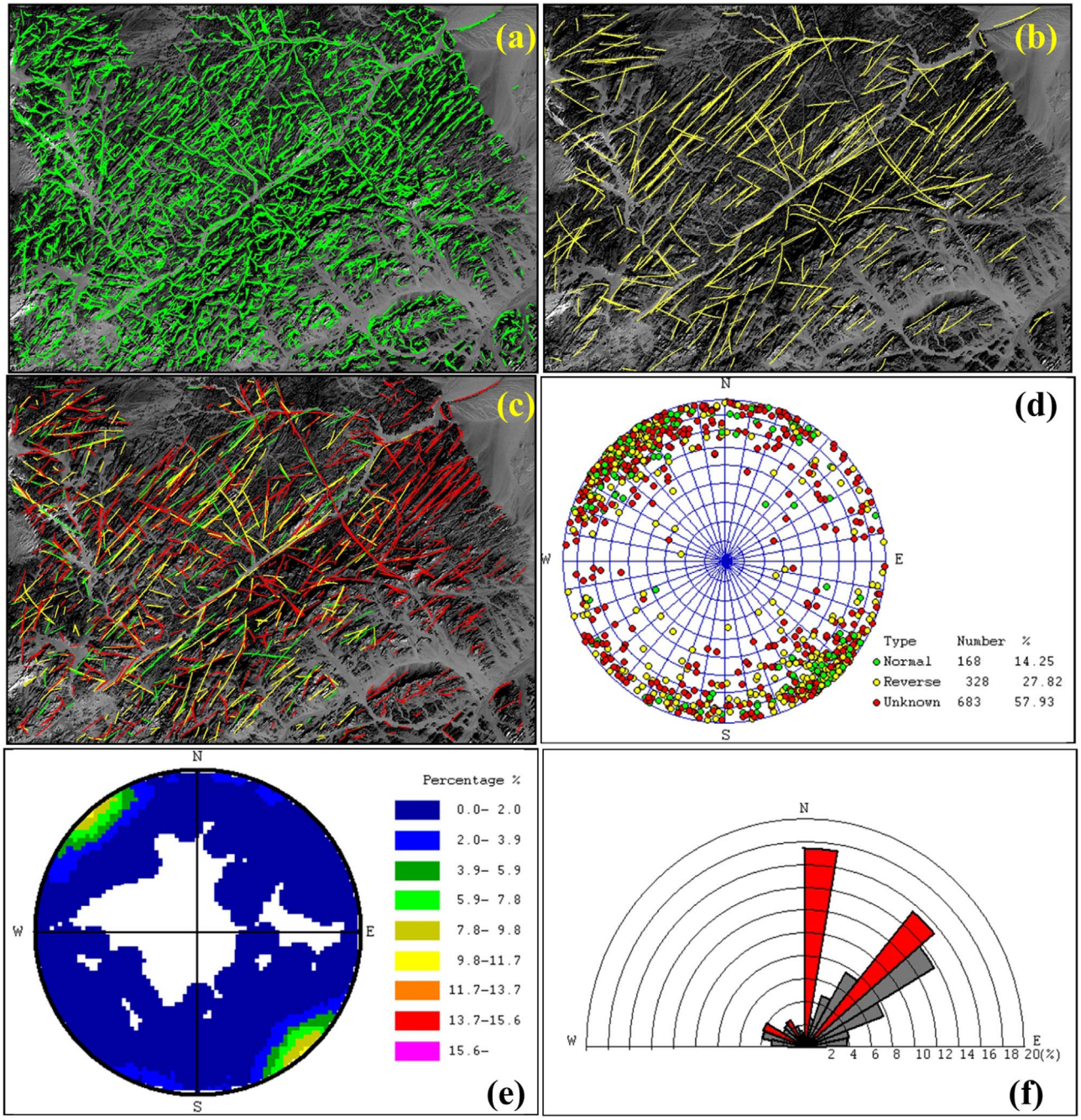

Fig. 6. Flow of LINDA using Landsat 7 ETM+ band 1 image (Fig. 4b) of first study area; (a) segments over band 1 image; (b) Bézier-smoothed lineaments; (c) BSP-smoothed lineaments with fault types (yellow: normal, green: reverse, and red: strike-slip); (d) distribution of poles of interpreted fracture- or fault-related planes with fault types; (e) pole density using Schmidt nets (lower hemisphere projection); (f) rose diagram for strikes of lineaments (For interpretation of the references to color in this figure legend, the reader is referred to the web version of this article.).

image use. Predominance of the NE trend in the dyke swarms is common to the two data sources and the lineaments of V-shaped valleys, but the second most common trend is different, i.e., N-S from DEM use and E-W from image use. N-S dykes are known to be one of dominant trends in the study area. Therefore, the geodynamic framework can be revealed more accurately by the multi-shaded DEM with LINDA.

4.2. Detection and characterization of faults

The second test area for verifying the performance of LINDA was a part of the South Eastern Desert of Egypt (Fig. 8; size 28 km × 24 km). Because the faults and their types in this area were investigated and mapped by Abd El-Wahed and Kamh (2010) (Fig. 8e), these were used as a reference for LINDA lineaments and fault modeling.

Summary statistics of segments detected in the shaded DEM and six-band images are compared in Table 3. The advantage of using the shaded DEM (Fig. 8a) is proven by this comparison, because the number, maximum and mean lengths of the DEM segments were maximized. More and longer lineaments may increase the concordance ratio of lineaments to real faults and fractures. Segments from the B1 image (Fig. 8c) were subordinate to those three properties. Then, the B1 segments were selected and compared with the DEM segments (Fig. 8b and d). Their most distinct difference between the two was that the two continuous segments trending E–W and N–S appeared in the southern and middle parts of the DEM segments, respectively, coin-

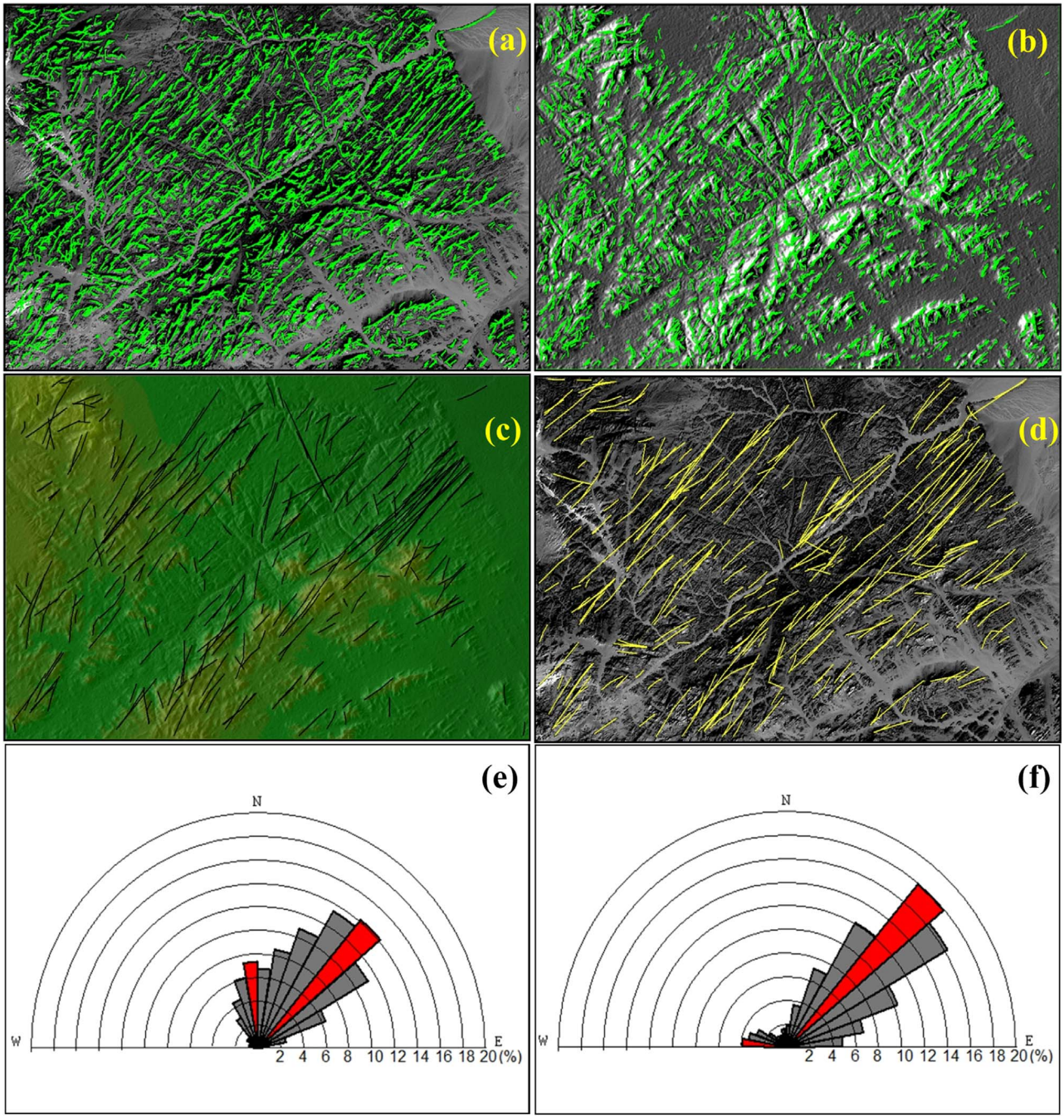

Fig. 7. Dykes detected from multi-shaded DEM by ATMDS (left) along with their (a) segments, (c) lineaments and (e) rose diagram, and from Landsat 7 band 1 image (right) along with their (b) segments, (d) lineaments and (f) rose diagram. (For interpretation of the references to color in this figure legend, the reader is referred to the web version of this article.)

cident with the mapped faults (Fig. 8e). Another difference was observed in the flat areas of wadis (ephemeral streams) and low-lying areas in the northeastern part, where image contrast was poor for all six bands. However, the ATMDS could enhance slight elevation change in such flat areas and LINDA could detect segments in the shaded DEM there. Consequently, the shaded DEM was more effective for lineament analysis than the satellite image data.

Next, locations, directions, and fault types of the lineaments formed by four or more grouped DEM segments were compared with reference data. This number was selected by referring to the general fault length in the study area. Although several faults that do not form clear topographic features did not appear in the lineament map, strong agreement of these components is confirmed by Fig. 8e. The main fault types are strike-slip as in the LINDA result, and the dip-slip faults (normal or reverse) are partially estimated. One capability of LINDA is accuracy of dip angle estimation, because differences of dip angles in the reference data are from 8° to 11° (average ± 5°) (Fig. 8e) and dip directions are largely correct.

Among the six Landsat bands, the segments were detected best in the visible blue B1 image (Table 2). The predominant direction of the Landsat-imagery segments and lineaments was NE in all bands, followed by NNE, NNW, and WNW trends. The DEM segments and lineaments had a different character, with the NNW, NNE and NE trends prominent in decreasing order (Fig. 9a and b). The rose diagrams of Fig. 9 were produced by counts in each azimuthal sector, and sectors of the trends are colored red. Generally, frequencies of NE directions perpendicular to the sun azimuth are frequent in the image result, which may contain image contrast bias from the illumination

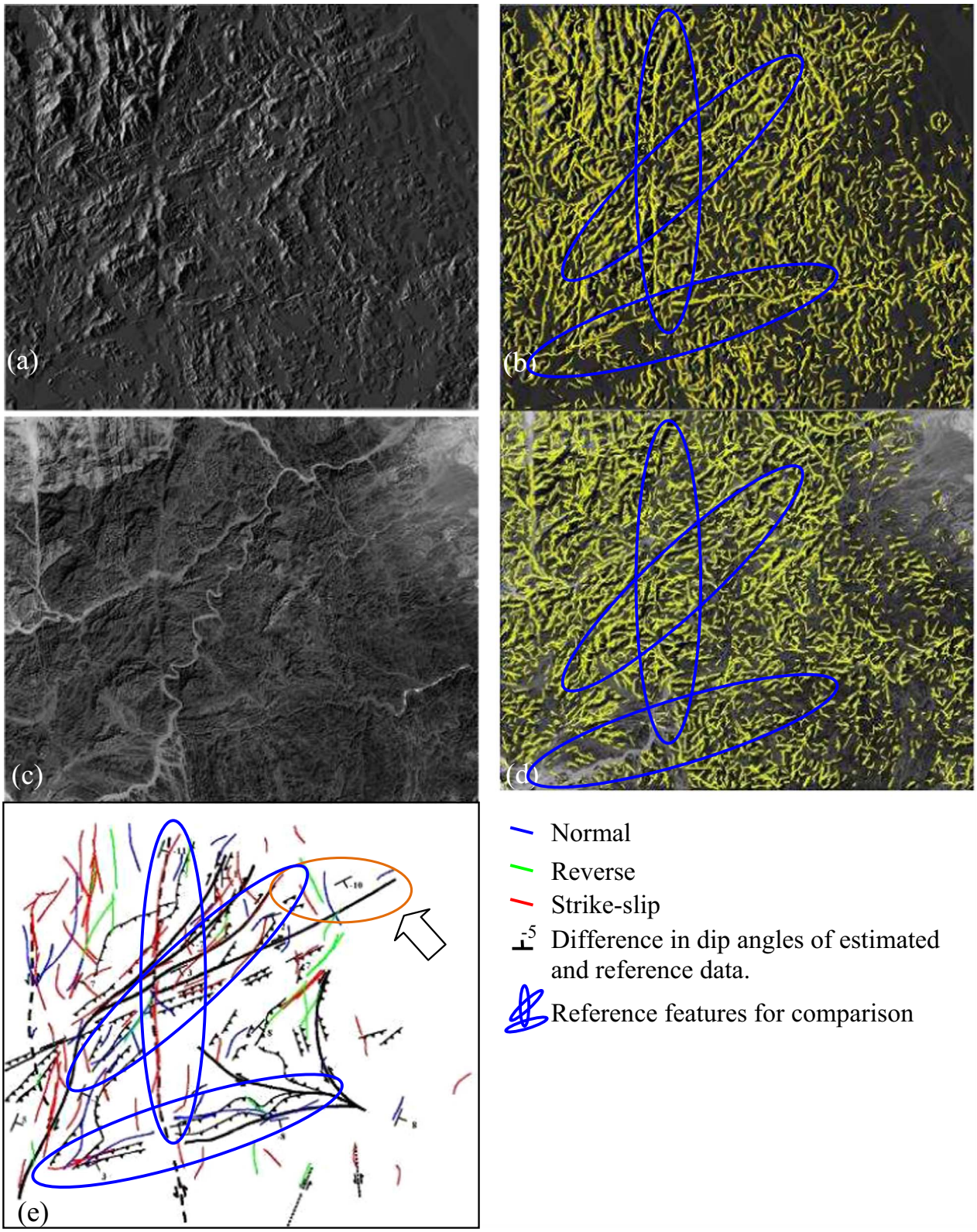

Fig. 8. Comparison of segments from DEM and satellite image data and verification of LINDA estimates of direction and fault type of lineaments. Test area is a part of the Eastern Desert of Egypt, bounded by 25°15'1.23"–25°28'15.49"N and 34°22'49.26"–34°39'44.51"E. (a) Multi-shaded DEM by ATMDS, (b) segments overlaid on it, (c) LANDSAT 7 ETM+ band 1 image, (d) segments detected from the image, and (e) lineaments formed from four or more grouped DEM segments and their estimated dip direction and angle and fault type (shown by three colors) from reference fault map (black) by Abd El-Wahed and Kamh (2010). The difference in dip angles between estimated and reference data is shown on the dip sign; the ellipse is an example to highlight the difference (e). (For interpretation of the references to color in this figure legend, the reader is referred to the web version of this article.)

effect. This problem is resolved by the DEM use, because the NNW directions that are parallel to the sun azimuth are dominant. However, the DEM result shows one disagreement, i.e., dominance of the NE directions is weak despite the presence of a long NE–SW fault (Fig. 8e). To compensate each the two limitations above, lineament directions from the DEM and B1 data were summed (Fig. 9c). The resultant rose

Table 3
Summary statistics of count and length (km) for segments detected from shaded DEM and six band images of LANDSAT 7 ETM+ (B1–B5 and B7) for South Eastern Desert test area shown in Fig. 8.

Data source	Count	Shortest	Longest	Mean	Standard deviation	Mode
DEM	9845	0.09	3.13	0.392	0.217	0.30
B1	9830	0.03	2.88	0.384	0.198	0.30
B2	9249	0.10	2.58	0.379	0.193	0.30
B3	8938	0.09	2.28	0.375	0.183	0.30
B4	8658	0.09	2.20	0.374	0.185	0.24
B5	8799	0.11	2.24	0.373	0.185	0.27
B7	8981	0.11	2.66	0.377	0.190	0.30

diagram depicts a feature similar to the reference fault data, in which the four most prominent trends (NE, NNE, NNW, and WNW) correspond to each other within a 10° difference (Fig. 9c and d). These trends also form the dominant structures in the basement crystalline terrain of Egypt (Masoud and Koike, 2011a). This suggests that the integration of lineament analyses using the DEM and satellite imagery can contribute to more detailed structural mapping than independent analysis. By use of a higher-resolution DEM, fracture-detection accuracy from small to large scale may be improved.

5. Conclusions

LINDA has been designed and developed as a user-friendly, interactive tool for automated detection of linear features, analyses, and visualization using multiple sources of grid data. The software has been used successfully in mapping local and regional lineaments and characterizing fracture and fault systems in many case studies in Egypt and Japan. This paper presented an implementation of a suite of tools programmed in VB and Fortran 90 for automation of these tasks. There is no software dedicated to lineament analysis using tools similar to the present study. VB and Fortran 90 provide suitable development environments for this type of software for the following reasons. Spatial analyses can be carried out using the Windows operating system, with which the majority of researchers are familiar. The use of LINDA does not require learning a programming environment. Embedding the analysis routines in Fortran 90 speeds execution. The relative simplicity of the VB language facilitates the development and version update of user-friendly graphical interfaces.

LINDA is automated in a one-step process that can execute all analyses with one mouse click and save time and effort. The detected lineaments are not biased in direction by the adaptive shading of grid data from multiple illumination directions. That bias has traditionally arisen from interactive setting of the azimuth and altitude of a one-directional illumination source. The strong capability for detecting segments satisfying the criteria of straight linearity along valley features, irrespective of shade intensities, was demonstrated using ATMDS shaded grid data and STA. Then, long lineaments were represented by concatenating short segments and smoothing their connection into a gentle curve, using the BSP technique. LINDA proved promising in discriminating between dykes and valley features. Features from the DEM were more frequent and longer than those detected using the remote sensing data, in particular, band 1. Linear

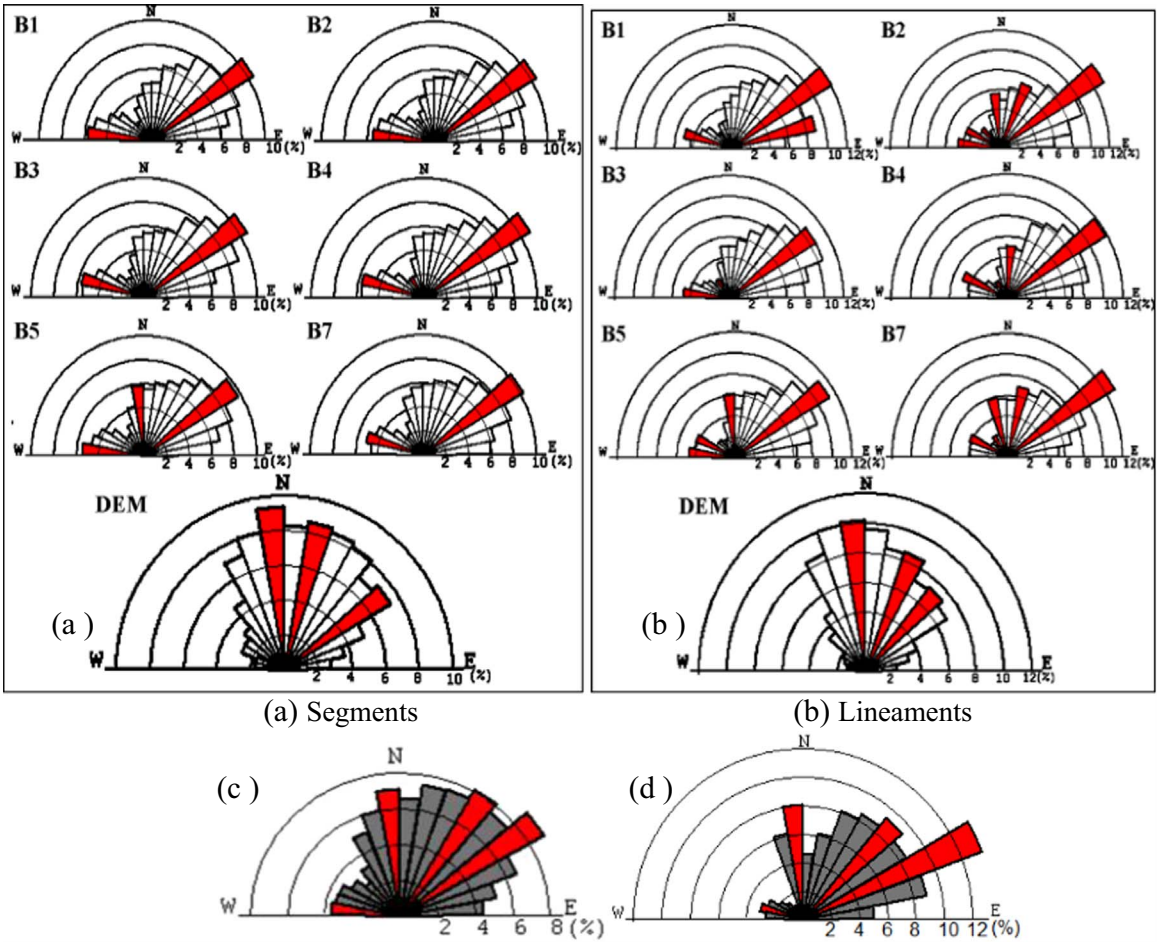

Fig. 9. Rose diagrams of (a) segments and (b) lineaments detected from multi-shaded DEM (Fig. 8a) and six band images of LANDSAT 7 ETM+, (c) summed lineaments from DEM and band 1 image, and (d) reference faults (Fig. 8e). Red-colored sectors of NE, NNE, NNW, and WNW denote prominent directions of major structures in basement crystalline terrain of Egypt (Masoud and Koike, 2011a). (For interpretation of the references to color in this figure legend, the reader is referred to the web version of this article.)

features from both sources can highlight, either individually or combined, the geodynamic framework in the region. Reference field-measured structural features clarified the applicability of LINDA for estimating the dip angle and detecting different fault types.

Future research will focus on enhancing the detection accuracy of linear features related to true fractures and faults using the grid data, by improving the detection criterion described in Section 2. Criteria in addition to the secondary differentiation must be defined, depending on fault topographies. Furthermore, application of the developed techniques to fine-scale and various types of potential field data (e.g., gravity and magnetic) using detailed structural information would be possible for localized areas. This can maximize reliability of the results, in particular for fault-type modeling, and make the validation process much easier.

LINDA is available at http://alaamasoud.tripod.com/id2.html or by contacting the corresponding author at alaa_masoud@science.tanta.edu.eg.

Acknowledgments

Authors are sincerely grateful to Prof. Gregoire Mariethoz, Editor-in-Chief of *Computers & Geosciences*, and to the two anonymous reviewers for their valuable comments and suggestions that helped us to improve the clarity of the manuscript. This research was partially supported by the Japan Science and Technology Agency (JST) and Japan International Cooperation Agency (JICA) through the Science and Technology Research Partnership for Sustainable Development (SATREPS).

Appendix A. : LINDA GUI components

File

The file menu enables reading and displaying text and bitmap data files in ASCII format and saving results in bitmap form. The resultant maps are used as backgrounds when displaying the segments/lineaments to validate location accuracy of the detected features, using various data sources. Data files of the DEM, shades, satellite image bands, and geology can be displayed with their image coordinates (widths and heights). Colors are assigned as grayscale for shaded grid data and satellite band imagery. For other inputs, blue, green, and red (BGR) color composites are used to represent grid values from the data.

Picture

The picture submenu enables shade blending, with color maps produced from the DEM and grid data, color composites of satellite band images, geologic maps, and other thematic maps used to render a three-dimensional view. The shading weight is adjusted from 0% to 100% using the alpha blending technique (Porter and Duff, 1984).

Lineament

This submenu represents the core LINDA component for detection, analysis, and display of segments and lineaments. Seven processes can be executed consecutively or separately. These are shading, segment tracing, refining, grouping, calculating normal vectors of surfaces and strike/dip of interpreted fracture- or fault-related planes, fault-type modeling, and point mapping (described below). In each step, input files are produced along with parameter files, and outputs are provided as text files. The resulting segments/lineaments can be displayed without smoothing, or smoothed using Bézier or BSP curves. Bézier smoothing is applied to lineaments before calculating orientation (strike and dip) of the interpreted fracture or fault plane. BSP is used after the calculation to smooth the lineaments using fault data.

Strikes of grouped segments can be displayed using a rose diagram only. Diagrams of strike, length, fault type, and Schmidt nets are used to render interpreted plane features. Rose diagrams can be constructed using the number, length, and normalized length per number. Strike, dip, and fault type of each plane can be rendered for different lineament lengths. List boxes are used to illustrate the strike and dip for investigating results. Strike quadrangle (StQ), angle (StA), and length (L) of segments in kilometers are displayed in the first three list boxes at right of the Lineament Analysis panel (Fig. 3), and the last six list boxes display values of StQ, StA, dip quadrangle (DQ), dip angle (DA), fault type (FT), and length (L) of lineaments in kilometers. Icons showing the meaning of these variables are displayed at top of the list boxes, with the categories explained in Section 3.2.

Point

The point submenu displays the segment/lineament centers and intersection points of multiple lineaments in the form of circles of various colors. The objective of the point function is to highlight intensely fractured zones.

Text editor

In this submenu, the user can open, edit, and save the input/output text data and parameter file.

Appendix B. Supplementary material

Supplementary data associated with this article can be found in the online version at http://dx.doi.org/10.1016/j.cageo.2017.06.006.

References

Abarca, M.A.A., 2006. Lineament Extraction from Digital Terrain Models: Case Study San Antonio del Sur Area, South-eastern Cuba 62. International Institute for Geo-Information Science and Earth Observation, Enschede, the Netherlands.

Abd El-Wahed, M.A., Kamh, S.Z., 2010. Pan-African dextral transpressive duplex and flower structure in the Central Eastern Desert of Egypt. Gondwana Res. 18 (2), 315–336.

Argialas, D.P., Mavrantza, O.D., 2004. Comparison of edge detection and Hough transform techniques for the extraction of geologic features. Proceedings of the ISPRS Congress 35(3B), 790–795.

Austin, J.R., Blenkinsop, T.G., 2008. The Cloncurry Lineament: geophysical and geological evidence for a deep crustal structure in the Eastern Succession of the Mount Isa Inlier. Precambrian Res. 163 (1–2), 50–68.

Bonetto, S., Facello, A., Ferrero, A.M., Umili, G., 2015. A tool for semi-automatic linear feature detection based on DTM. Comput. Geosci. 75, 1–12.

Dawoud, M., Eliwa, H.A., Traversa, G., Attia, M.S., Itaya, T., 2006. Geochemistry, mineral chemistry and petrogenesis of a Neoproterozoic dyke swarm in the north Eastern Desert, Egypt. Geol. Mag. 143, 115–135.

Fichler, C., Rundhovde, E., Olesen, O., Saether, B.M., Ruelatten, H., Lundin, E., Dore, A.G., 1999. Regional tectonic interpretation of image enhanced gravity and magnetic data covering the mid-Norweigian shelf and adjacent mainland. Tectonophysics 306 (2), 183–197.

Goren, L., Fox, M., Willett, S., D., 2014. Tectonics from fluvial topography using formal linear inversion: theory and applications to the Inyo Mountains, California. J. Geophys. Res.: Earth Surf. 119 (8), 1651–1681.

Hassanein, H., Soliman, Kh, 2008. Aeromagnetic data interpretation of Wadi Hawashiya area for identifying surface and subsurface structures, North eastern desert, Egypt. J. King Abdulaziz Univ.: Earth Sci. 20 (1), 117–139.

Koike, K., Nagano, S., Kawabata, K., 1998. Construction and analysis of interpreted fracture planes through combination of satellite-derived lineaments and digital elevation model data. Comput. Geosci. 24 (6), 573–583.

Koike, K., Nagano, S., Ohmi, M., 1995. Lineament analysis of satellite images using a Segment Tracing Algorithm (STA). Comput. Geosci. 21 (9), 1091–1104.

Kudo, T., Yamamoto, A., Nohara, T., Kinoshita, H., Shichi, R., 2004. Variations of gravity anomaly roughness in Chugoku district, Japan: relationship with distributions of topographic lineaments. Earth Planets Space 56 (5), e5–e8.

Masoud, A.A., Koike, K., 2006. Tectonic architecture through LANDSAT-7 ETM+/SRTM DEM-derived lineaments and relationship to the hydrogeologic setting in Siwa Region, NW Egypt. J. Afr. Earth Sci. 45 (4–5), 467–477.

Masoud, A.A., Koike, K., 2011a. Auto-detection and integration of tectonically significant lineaments from SRTM DEM and remotely-sensed geophysical data. ISPRS J. Photogramm. Remote Sens. 66 (6), 818–832.

Masoud, A.A., Koike, K., 2011b. Morphotectonics inferred from the analysis of topographic lineaments auto-detected from DEMs: application and validation for the Sinai Peninsula, Egypt. Tectonophysics 510 (3–4), 291–308.

Milbury, A.E.C., Smrekar, S.E., Raymond, C.A., Schubert, G., 2007. Lithospheric structure in the east region of Mars'dichotomy boundary. Planet. Space Sci. 55 (3), 280–288.

Nossair, L.M., 1987. Structural and Radiometric Studies on Gabal Gharib area, North Eastern Desert, Egypt. Fac. Sci., Alexandria University, Egypt, (Ph.D. Thesis) (Unpub.).

Oakey, G., 1994. A structural fabric defined by topographic lineaments: correlation with Tertiary deformation of Ellesmere and Axel Heiberg Islands, Canadian Arctic. J. Geophys. Res. 99 (B10), 20311–20321.

Porter, T., Duff, T., 1984. Compositing digital images. Comput. Graph. 18 (3), 253–259.

Raghavan, V., Masumoto, S., Koike, K., Nagano, S., 1995. Automatic lineament extraction from digital images using a segment tracing and rotation transformation approach. Comput. Geosci. 21, 555–591.

Ramli, M., Yusof, N., Yusoff, M., Juahir, H., Shafri, H., 2010. Lineament mapping and its application in landslide hazard assessment: a review. Bull. Eng. Geol. Environ. 69, 215–233.

Rowland, J.V., Sibson, R.H., 2004. Structural controls on hydrothermal flow in a segmented rift system, Taupo Volcanic Zone, New Zealand. Geofluids 4, 259–283.

Roy, S., Sahu, A.S., 2015. Quaternary tectonic control on channel morphology over sedimentary low land: a case study in the Ajay-Damodar interfluve of Eastern India. Geosci. Front. 6 (6), (927-046).

Šilhavý, J., Minár, J., Mentlík, P., Sládek, J., 2016. A new artefacts resistant method for automatic lineament extraction using Multi-Hillshade Hierarchic Clustering (MHHC). Comput. Geosci. 92, 9–20.

Soto-Pinto, C., Arellano-Baeza, A., Sánchez, G., 2013. A new code for automatic detection and analysis of the lineament patterns for geophysical and geological purposes (ADALGEO). Comput. Geosci. 57, 93–103.

Stern, R.J., Gottfried, D., Hedge, C.E., 1984. Late Precambrian rifting and crustal evolution in the northeast Desert of Egypt. Geology 12, 168–172.

Stern, R.J., Voegeli, D.A., 1987. Geochemistry, geochronology, and petrogenesis of a Late Precambrian (=590 Ma) composite dike from the North Eastern Desert of Egypt. Geol. Rundsch. 76, 325–341.

Süzen, M.L., Toprak, V., 1998. Filtering of satellite images in geological lineament analyses: an application to a fault zone in Central Turkey. Int. J. Remote Sens. 19 (6), 1101–1114.

Tripathi, N., Gokhale, K., Siddiqu, M., 2000. Directional morphological image transforms for lineament extraction from remotely sensed images. Int. J. Remote Sens. 21, 3281–3292.

Vasuki, Y., Holden, E., Kovesi, P., Micklethwaite, S., 2014. Semi-automatic mapping of geological structures using UAV-based photogrammetric data: an image analysis approach. Comput. Geosci. 69, 22–32.

Vaz, D.A., Di Achille, G., Barata, M.T., Alves, E.I., 2012. Tectonic lineament mapping of the Thaumasia Plateau, Mars: Comparing results from photointerpretation and a semi-automatic approach. Comput. Geosci. 48, 162–172.

Wang, J., 1993. LINDA - a system for automated linear feature detection and analysis. Can. J. Remote Sens. 19 (1), 9–21.

Warner, T.A., 1997. Integration of remotely sensed geobotanical and structural methods for hydrocarbon exploration in West-central West Virginia. Final report for DOE-sponsored Research Contract DE-FG21-95MC32159. Morgantown, WV, 55pp.

Wołosiewicz, B., 2016. Morphotectonic control of the Białka drainage basin (Central Carpathians): insights from DEM and morphometric analysis. Contemp. Trends Geosci. 5 (1), 61–82.